21

Integration of Satellite Imagery, Geology and Geophysical Data

Andreas Laake
WesternGeco Cairo
Egypt

1. Introduction

Satellite imagery is a large scale surface geological mapping too, which offers the unique opportunity to investigate the geological characteristics of remote areas of the earth surface without the need to access the area on the ground. The resolution of the technique is limited by the resolution of the imagery. This chapter explains how geological information can be extracted from satellite imagery and how this information can be merged with geological and geophysical data to build consistent geological models for the surface and subsurface. On the one hand, the interpretation of satellite imagery can generate start models prior to the start of geophysical surveys. On the other hand, geological and geophysical data can calibrate models derived from satellite imagery.

2. Methodology

When studying the shape of the earth surface in connection with the rock layers and their deformation by tectonic forces, we often notice a correlation between shapes and structures at the surface and in the subsurface (Short and Blair 1986). This opens the opportunity to map the characteristics of the surface and infer characteristics of the subsurface. We can describe the surface by its shape and by its structure. The surface shape depends on topography, terrain gradient and surface lithology, which we call **geomorphological properties**. The surface structure is determined by lithological boundaries and fracture zones outcropping at the surface, which we call **litho-structural properties**. Fracture zones can also be inferred from the characteristics of recent or paleo-drainage (Short and Blair 1986). Geomorphology and litho-structure allow building a **static geological model**. If information is available about the elevation change with time, then the statics model can be expanded into a **dynamic geological model**. Figure 1 gives an over of the building blocks for geological model building.

We illustrate the methodology at a simple layer-cake geological model which is deformed by a vertical fault (fig. 2). The surface is formed by a soft sandstone layer resting on a hard limestone layer. These two layers form the near-surface. We call the layers between the bottom of the near-surface and the top of the basement subsurface. Prior to the deformation by the fault only the soft sandstone was visible at the surface. The fault has lifted part of the layer package and exposed the near-surface sandstone and limestone layers at the fault plane and made them accessible for mapping by satellites.

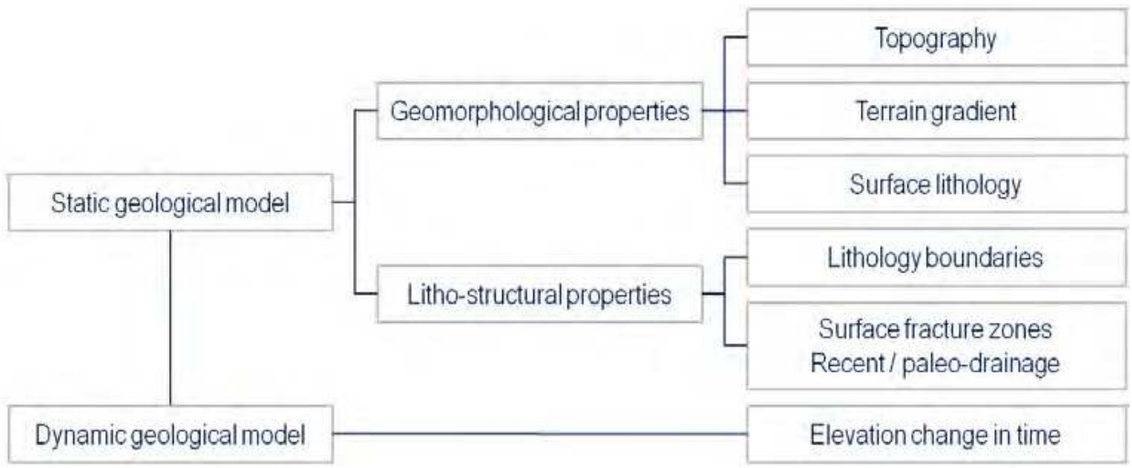

Fig. 1. Building blocks of near-surface and subsurface geological models

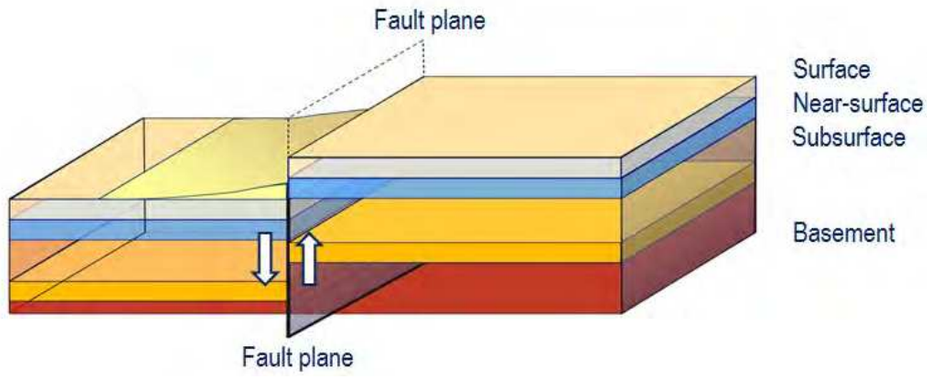

Fig. 2. Correlation of surface shape and subsurface geology

3. Satellite imagery

Earth observation satellites map the physical properties of the earth surface and near-surface. In the context of geological mapping we distinguish two types of electro-magnetic methods (see figure 3) :

- **passive optical methods**: use the sunlight as the source and measure the reflectance of the earth surface in the visible and infrared spectral bands. We used Landsat 7 ETM+ and the ASTER instrument from the Terra satellite.
- **active microwave radar methods**: use a microwave source onboard of the satellite and measure the back-scatter from the earth. We used Radarsat-1 and the radar sensor from the Shuttle Radar Tomographic Mission (SRTM).

Details about the acquisition and processing are provided among others by the USGS (2011) and Short (2010). For an introduction into the interpretation of satellite imagery see Sabins (1996). The **visible imagery (VIS)** covers the colors blue, green and red and provides information about water features, infrastructure and landuse as well as limited information about selected rock types. Infrared imagery is split into three classes : **very near infrared (VNIR)**, which detects specifically vegetation; **short wave infrared (SWIR)** which is the best

option for the discrimination of sedimentary rocks; and finally **thermal infrared** (TIR). The thermal infrared radiation from the earth surface represents the property of the surface material to convert the solar spectrum into heat radiation. We distinguish between a warm response from dark materials such as non-sedimentary rocks and cool response from ground moisture or voids, where evaporation absorbs energy. In general optical imagery does not penetrate the earth surface.

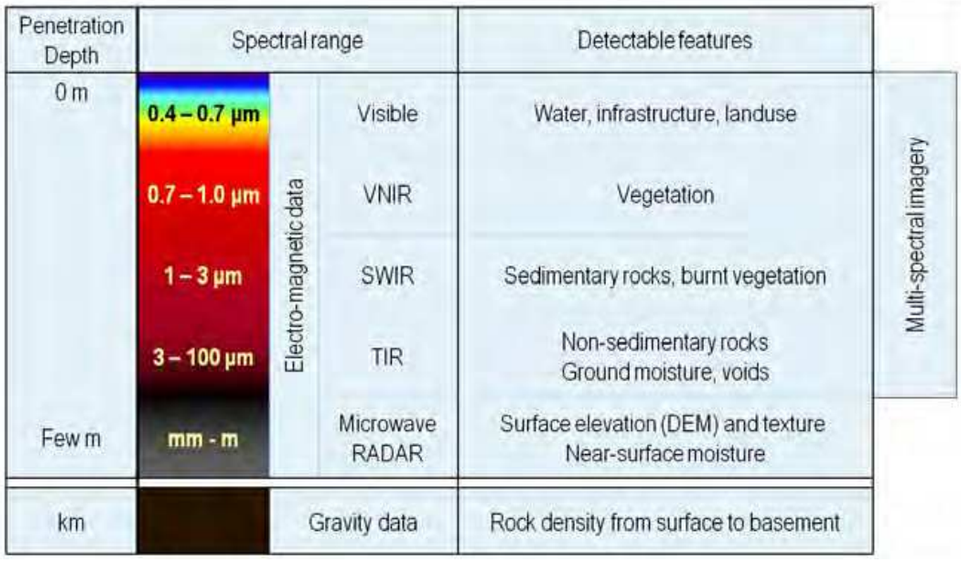

Fig. 3. Spectral overview of electro-magnetic satellite imagery

Microwave radar uses electro-magnetic waves in the mm to m range. At hard surfaces microwaves are almost completely back-scattered. Their travel time can be used to determine the distance between the satellite and the surface, which is used to generate digital elevation models (DEM). For soft, non-conductive surfaces the microwaves penetrate into the subsurface; the back-scattered signal is generated from volume scatter in the subsurface.

A special application of microwave radar is the estimation of **gravity anomalies**. Sandwell and Smith (2009) have studied anomalies in the orbits of radar satellites and inferred Bouguer gravity anomalies using a geoid model. These gravity anomalies can be interpreted for the thickness of the sedimentary cover above the crystalline basement.

The following examples illustrate the information obtainable from the various satellite imagery sets. Figure 4 shows an example of multi-spectral data from ASTER for each range : visible (fig. 4.a), short wave infrared (fig. 4.b) and thermal infrared bands (fig. 4.c) of the island of Bahrain with a colour scale from blue (low reflection intensities) via green and yellow to red (high intensities). The visible green band penetrates water for a few meters (blue shades). It is relatively insensitive to different rock types (red shades). The short wave infrared band does not penetrate water and therefore shows uniform blue color, whereas it allows the discrimination of the different rock types in the oval anticlinal structure covering most of the island (yellow and red shades). The thermal infrared band shows the thermal properties such as warm response from the built-up areas (dark red). Cool response (greenish areas in the coastal areas) is observed for wet coastal salt flats called sabkha.

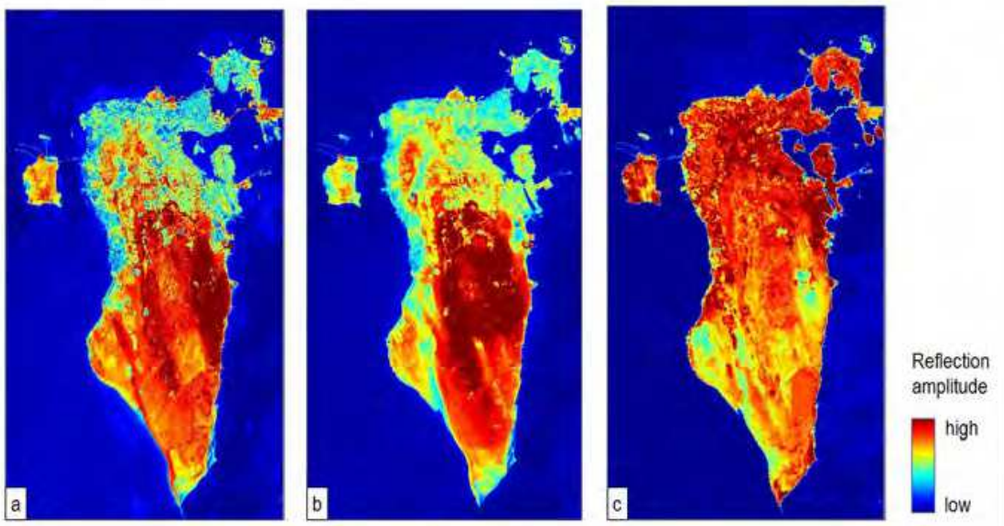

Fig. 4. Examples for optical satellite imagery from ASTER: a – visible blue, b – short wave infrared, c – thermal infrared [after Laake et al. 2006]

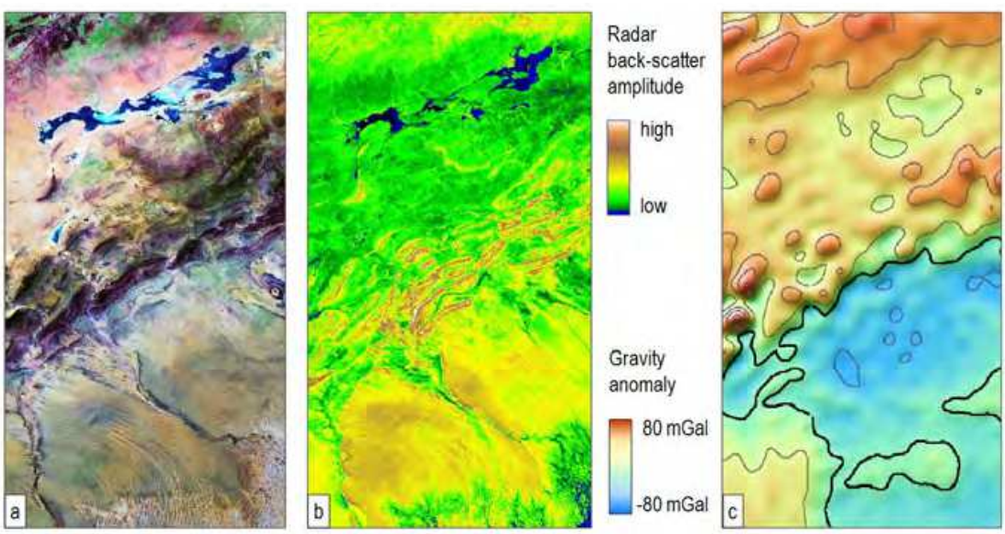

Fig. 5. Examples for optical and radar satellite imagery: a – optical data [Landsat 742 RGB] for comparison, b – radar scatter intensity [Radarsat-1], c – gravity anomaly derived from radar

The examples for microwave radar data show the Atlas area in Algeria. For orientation we have supplied a Landsat 742 RGB image (fig. 5.a), which shows mountain ranges (dark purple), gravel planes (yellow-gray), salt lakes (blue) and vegetation (green). The radar back-scatter intensity from Radarsat-1 (fig. 5.b) is displayed from blue (total absorption in conductive salt brine) via intermediate volume back-scatter (green and yellow) to strong surface back-scatter from hard rock (brown and white).

Figure 5.c shows the gravity anomaly inferred from radar satellite imagery. Negative anomalies correspond to low density rocks as from thick sedimentary cover at the foot of the

Atlas mountains whereas positive anomalies correlate with dense metamorphic and basement rocks in the Atlas ranges.

4. Extraction of information from satellite imagery

Satellite imagery is provided as sets of digital images, one image for each spectral band. Each image displays the measured values as intensity. The information contained in the satellite imagery can be extracted using either single bands or combinations of bands**. Single bands** are usually displayed as maps coding measured amplitude as colour.
Figure 6 shows radar data from the very dry desert in south-west Egypt : radar data from the shuttle radar tomographic mission (SRTM, Jarvis et al., 2008) interpreted for a DEM using topographic colour coding, i.e. green for low elevations, yellow to brown for high ground (fig. 6.a). Raw radar data from Radarsat-1 reveal high amplitudes from the back-scatter at hard sandstone (white and brown colors in fig. 6.b). Low radar back-scatter (fig. 6.c) correspond to volume back-scatter from microwaves penetrating sand sheets. They reveal buried paleo-rivers (blue colors in fig. 6.c) following the interpretation by El-Baz and Robinson (1997) and Robinson et al. (2007).

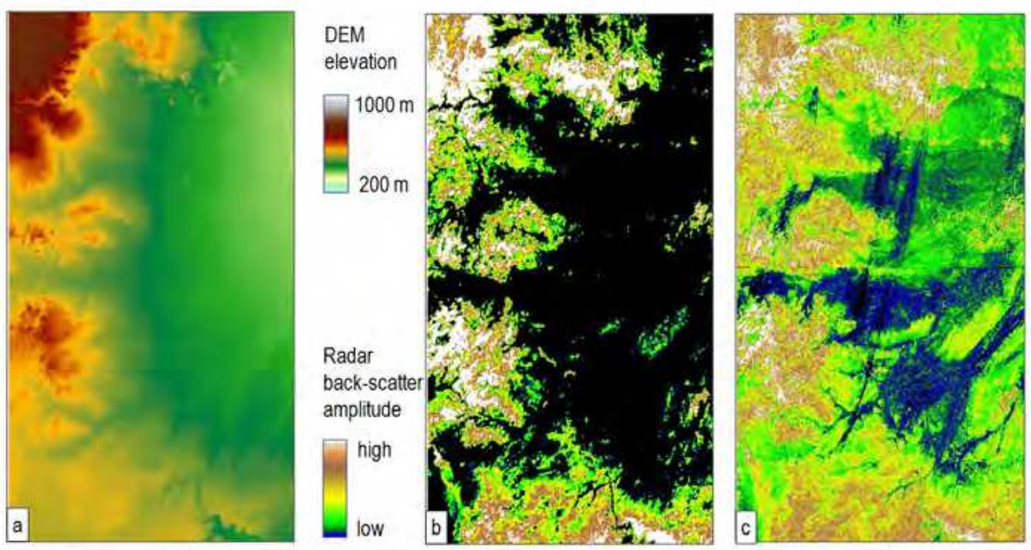

Fig. 6. Single band data examples : a – radar based digital elevation model [SRTM DEM], b – high intensity radar data [Radarsat-1], c – low intensity radar data [Radarsat-1]

Dual band images use combinations of two bands from Landsat for the north-western desert in Egypt (fig. 7) thereby enhancing subtle features in the data that would not be imaged by a single band alone. The ratio of the infrared bands 7 and 4 (fig. 7.a) highlights for example clay minerals which fill karst holes (red and cyan) in an otherwise homogeneous limestone plateau (dark blue). The band difference of the very near infrared band 4 and the green band 2 for the same area highlights difference in lithology between the pure limestone (yellow to red) and the more sandy cover (blue tones) towards the top of the image (fig. 7.b).
Multi-band images use three or more bands combined in continuous colour or red-green-blue (RGB) images. RGB images provide significantly more shades than single or dual band images: for 8 bit imagery an arithmetic combination of 3 bands provides 256 shades whereas an RGB image offers 16.8 million colors (Guo et al., 2008).

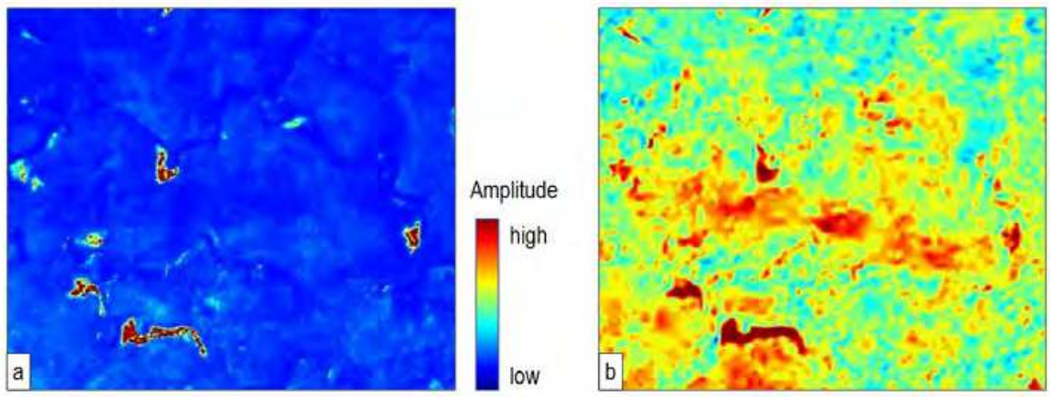

Fig. 7. Dual band data examples: a – band ratio [Landsat 7/4], b – band difference [Landsat 4-2] for the same area

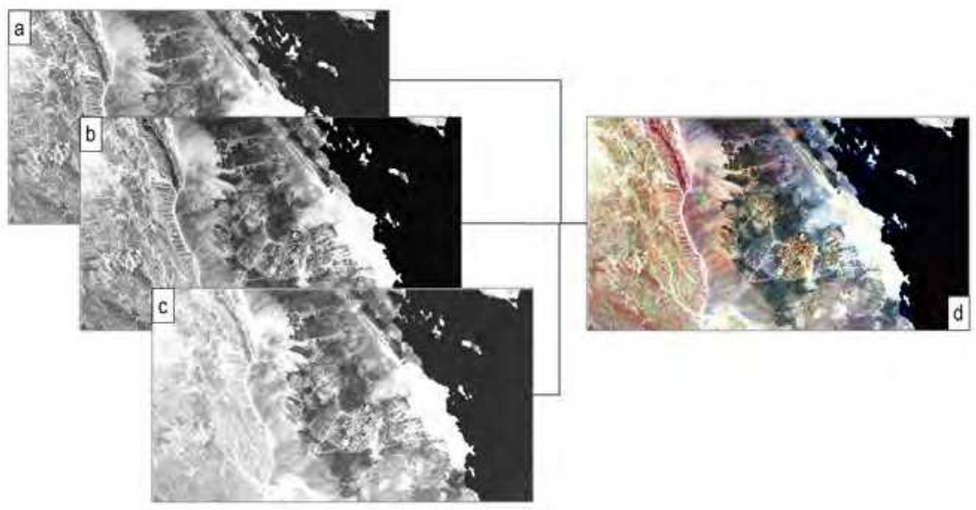

Fig. 8. Multi-band data example : merge of single band data (a to c) into RGB image (d) [Landsat 742 RGB]

To illustrate this we study an example from the southern Red Sea Mountains and the adjacent coastal area in south-east Egypt (fig. 8). The raw input bands (fig. 8 a-c) show only marginally different signatures for the very different rock types, whereas the multi-band RGB image (fig. 8.d)distinguishes clearly between the basement rocks (dark), the Mesozoic clastic sedimentary rocks (yellow tones), coastal carbonates (white) and the sea (black).

5. Integration of satellite imagery and geology

In this section we describe techniques to extract geological information from satellite imagery and how to integrate this information with geological data. Satellite imagery is interpreted for surface topography and lithology as well as for surface and subsurface structure with the goal of generating geological models for the near-surface and subsurface (Laake and Insley, 2007, and Laake et al., 2008). The techniques are illustrated through a series of case histories starting with simple layer-cake geology.

5.1 Layer-cake geology (Qattara Depression, Egypt)

The surface north of the Qattara depression in Egypt is dominated by flat layering of hard and soft rocks at the surface (fig. 9). The raw DEM (fig. 9.a) shows a platform (yellow), which is located between rough hills (brown tones) and a sharp escarpment towards the Qattara Depression (green to blue). The terrain classification map (fig. 10.c) allocates the different elevations to three classes. The lithological analysis of the multi-spectral image (fig. 9.b) allows a clear separation into rock types : two types of limestone (blue tones), two types of sandstone (yellow to orange) and evaporites of the sabkha at the bottom of the depression (cyan).

Ideally the surface lithology interpretation is validated in the field (see fig. 10) using GPS tracked lithological analysis. The combination of terrain classification and lithology suggests that the plane represents the top of the sandstone formation, which continues also below the limestone layers, which form the higher ground. We will use this geological model to estimate statics for seismic data processing in section 5.

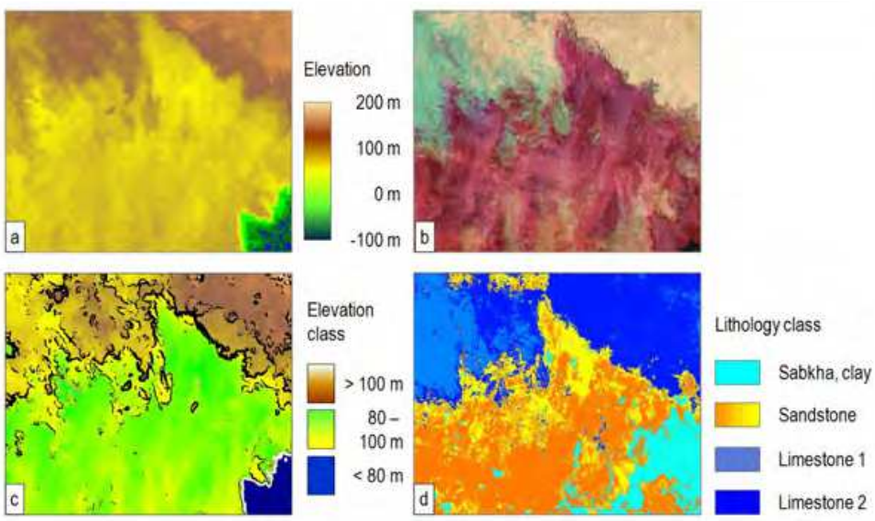

Fig. 9. Layer-cake geology near Qattara Depression, Egypt : a – digital elevation model [SRTM DEM], b – multi-band satellite image [ASTER 631 RGB], c – terrain classification map, d – lithology map [Cutts and Laake 2009]

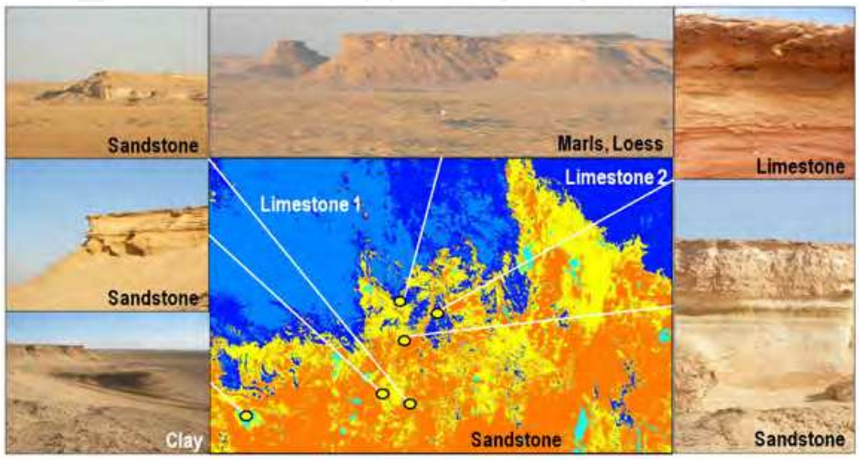

Fig. 10. Validation of lithology map in the field [after Coulson et al. 2009]

5.2 Anticline (Awali, Bahrain)

The outline of the island of Bahrain is determined by the topographical and lithological structure of the Awali anticline (fig. 11). We use satellite imagery from the ASTER sensor for the discrimination of clastic and carbonatic rocks (Laake et al., 2006).

The continuous colour image from short wave infrared and visible bands (ASTER 631 RGB in fig. 11.a) allows discriminating the coastal farmland in the north (green) from the carbonates of the anticline (purple tints) and coastal sabkha (cyan). The structure of the anticline can be delineated using the difference of visible and short wave infrared data (fig. 11.b), which can be traced even in the built-up area of Manama city in the north. The outer contour of the anticline appears highlighted in the west through the strong signature of the coastal sabkha (dark red). Draping the continuous colour image over the vertically exaggerated DEM generates a strong structural impression, which is useful for structural interpretation (fig. 11.c).

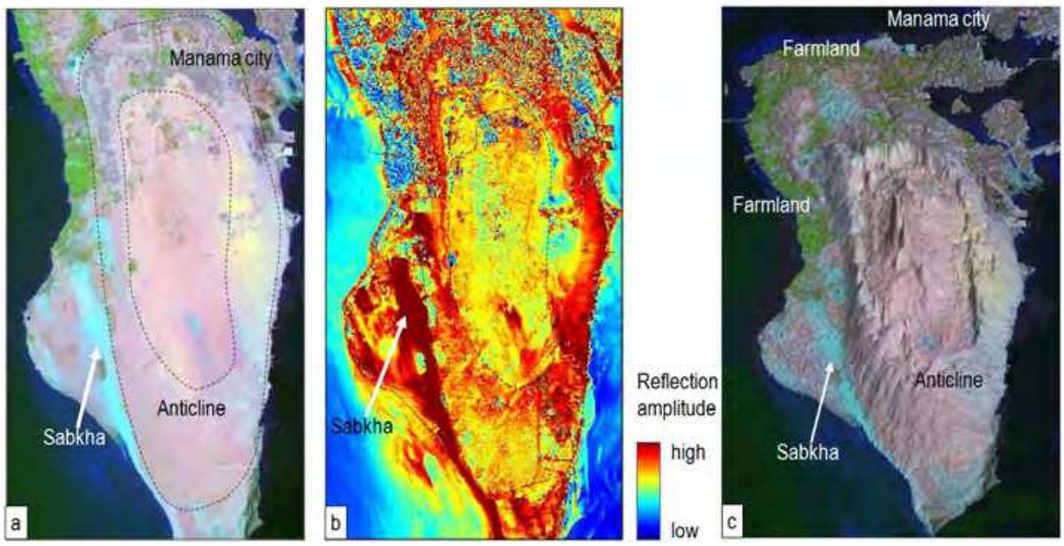

Fig. 11. Anticlinal structure of Awali, Bahrain : a – multi-spectral image [ASTER 631 RGB], geological structure from band difference image [ASTER visible minus short wave infrared], c – rendering of multi-spectral image on DEM [after Laake et al. 2006]

5.3 Mapping of basins from gravity and radar data (Illizi Basin, Algeria)

The mapping of basins from satellite imagery is the only remote sensing technique which infers deep geological structures. Bouguer gravity anomalies inferred from satellite radar data give an indication of the thickness of the sedimentary cover above the basement. However, this interpretation requires additional information for example from magnetic data to constrain the model. Following the concept of geomorphology, which correlates surface and subsurface geology and litho-structure, surface structural lineaments can be used to infer subsurface structures.

In figure 12 we show structural maps from satellite imagery for the Illizi Basin, which is indicated by the black continuous line in each figure. The lithology image (Landsat 742 RGB, fig. mapping 12.a) distinguishes dark paleozoic limestone (blue tones) and Mesozoic clastics (brown tones), which surround recent sand dunes (yellow). The geomorphological map (fig. 12.b) highlights the litho-structural boundaries, which are co-located with topographic

ridges. Satellite gravity data (fig. 12.c) reveal a basin (blue). The combination of surface geomorphology and gravity (fig. 12.d) gives an indication of the basin outline.

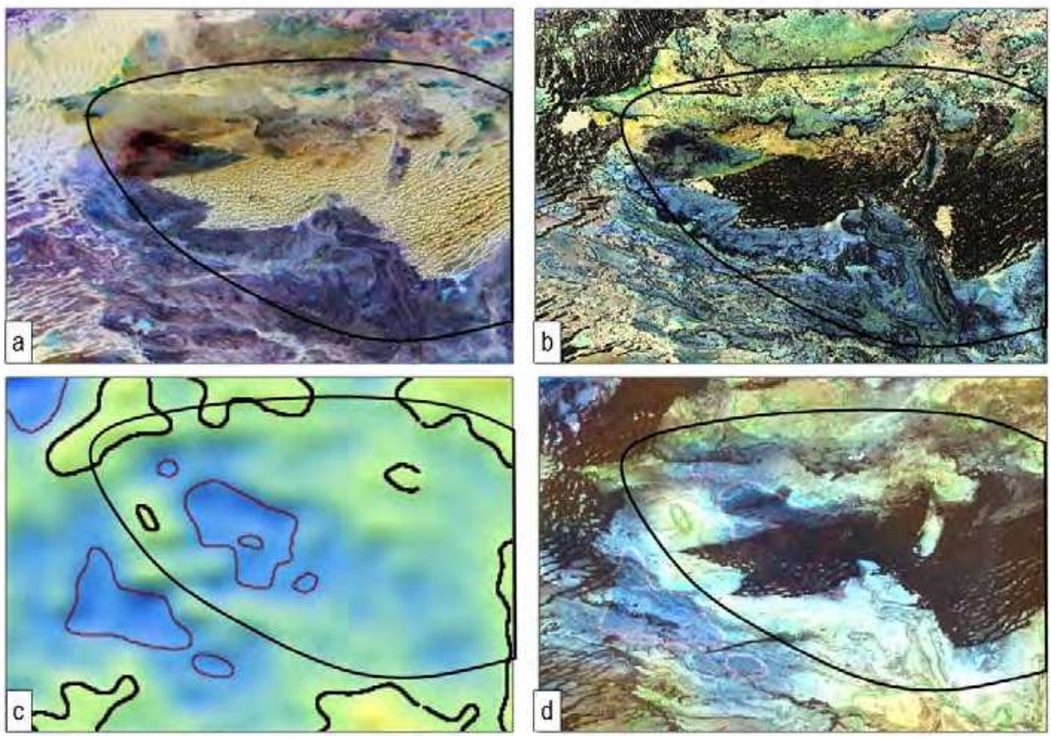

Fig. 12. Basin mapping of Illizi basin, Algeria: a – multi-spectral image (Landsat 742 RGB], b – geomorphological map [SRTM DEM, Landsat 742 RGB], c – gravity anomaly derived from radar, d – overlay of geomorphology on gravity data

5.4 Mapping of fracture zones below sand cover (Gilf Kebir, Egypt)

When sand dunes cover fracture zones in the near-surface, satellite radar data can map ancient river courses, from which fracture related weak zones in the near-surface can be derived (fig. 13). We start with the outcrops of faults in the hard rock surrounding the sand dune field mapping straight valleys in the hard sand stone. The topography of the study area (fig. 13.a) is composed of the flat Gilf Kebir plateau (brown tones) with gentle slopes (yellow) and a large plane (green to white). This corresponds to a surface lithology (fig. 13.b) of hard sandstones (greenish-brown) and basement rocks (dark brown) as well as belts of sand dunes (white), which are locally discoloured by hematitic iron (purple). The shape of the escarpment and the valleys intersecting the Gilf Kebir plateau reveal fairly straight fault lines (black lines). Below sand neither topographical nor optical satellite imagery can reveal buried fracture zones. Therefore we use satellite radar which can penetrate dry sand for up to 20 m to map the clay contained in buried paleo-river beds. The radar data (fig. 13.c) do not only map the fracture zones in the sandstone of the plateau (brown lineaments), it also shows W-E and SW-NE trends in the paleo-river courses (low radar intensities in blue) which continue from the lineaments in the rock outcrops. The overlay of the paleo-river courses from radar data on the geomorphology delineates the outcropping fracture zones across all terrains (fig. 13.d).

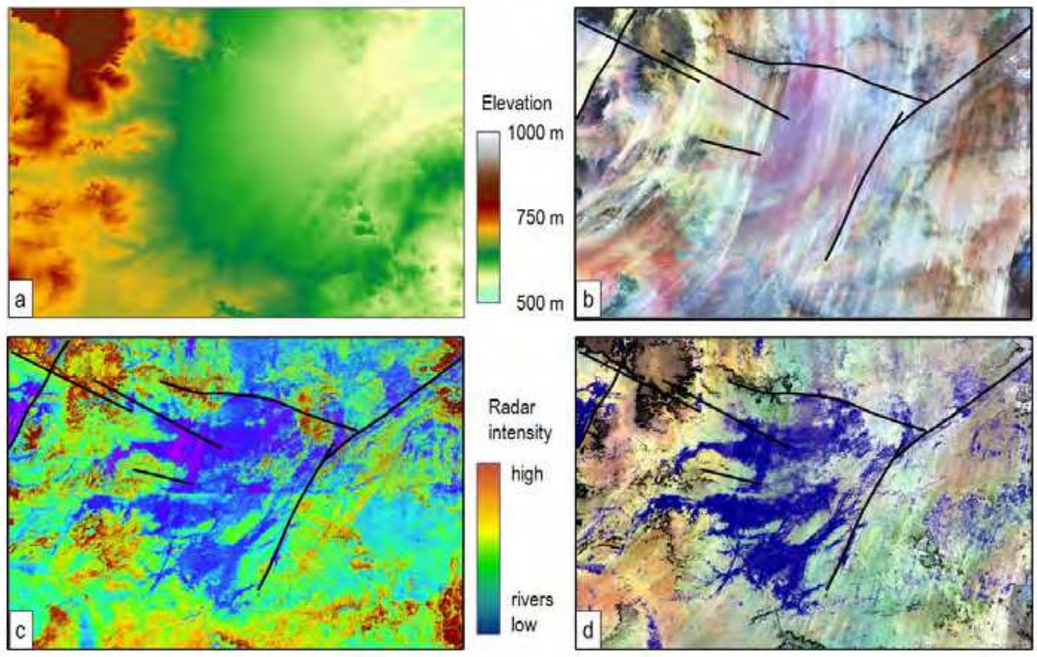

Fig. 13. Structural delineation from radar data close to Gilf Kebir, Egypt: a – DEM, b – multi-spectral image [Landsat 742 RGB], c – low intensity radar data [Radarsat1], d – merge of radar data with geomorphology. Faults indicated by lines.

5.5 Mapping of glacial moraine structures (Pechora Basin, Russia)

The last case study concerns the mapping of post-glacial structures in the Pechora basin in northern Russia using vegetation and water features as indicators; the lithology is not exposed in the study area. The structures studied comprise different types of moraines as well as drainage features in front of the glaciers (Laake 2009, Astakhov et al. 1999). We distinguish terminal and lateral moraines, which are composed of gravel and glacial till, from ground moraines, which are characterized by undulating terrain. Moraine ridges are often drier than the surrounding terrain because the elevated gravels cannot support a shallow water table. In contrast to this, ground moraines deposit more glacial till, which provides the basis for a shallow water table with very wet terrain and lakes. Significant differences in the ground moisture attract different plant species, which can be distinguished by their different response in the very near infrared and visible bands of satellite imagery. The topography allows delineating of the lateral and terminal moraines as long as they are still elevated above the surrounding plane (fig. 14.a).

Rendering the geomorphological map on the DEM in 3D improves the detection of these moraines. The location of lakes, which is indicative of ground moraines, is obtained from the landuse analysis of short wave infrared and visible green data. (fig. 14.c). The combination of all maps yields a clear delineation of the glacial moraines particularly when rendered in 3D (fig. 14.d). In this case four glacial stages can be interpreted (numbers in fig. 14) : an initial stage where the entire area was covered by a thick ice shield (1), which deposited ground moraines over the entire study area. The second (2) and the third (3) phase comprise two distinguishable glaciers, where the glacier from phase two created the partly broken moraine wall in the west. The glacier in phase three covered the centre of the study area

thereby partly levelling the lateral moraines from phase two. After melting, this glacier left the huge Lake Komi between the lateral and terminal moraines, which forms an extensive swamp today. The final glacier advance (4) covered only the northern third of the study area, leaving an irregular line of terminal moraines and extensive planes of ground moraines behind.

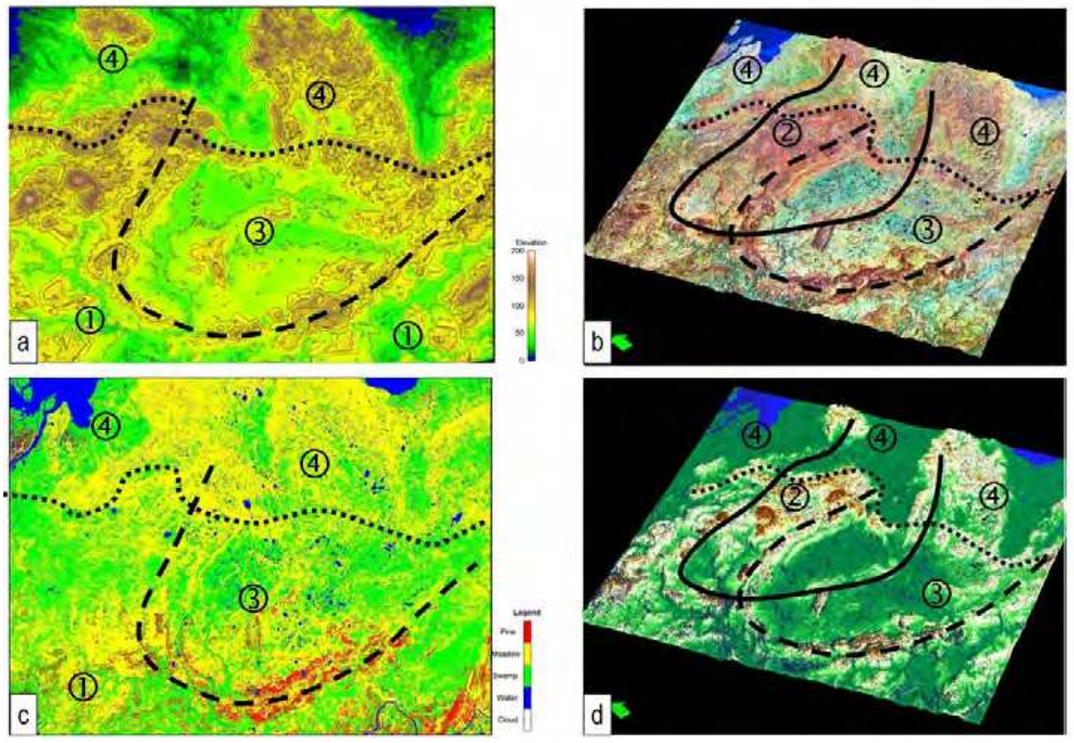

Fig. 14. Identification of glacial structures in Pechora basin, Russia: a – DEM [SRTM DEM], b – rendering of geomorphological map in 3D, c – landuse classification from Landsat, d – interpretation of geomorphology for glaciers and moraines [after Laake 2009]

6. Integration of satellite imagery and geophysics

The geological information extracted from satellite imagery can be used to build geological models from basin scale (several 10^5 sqkm) to survey scale (few 10^3 sqkm) well before any geophysical data are acquired on the ground. These models can be used for the estimation of logistic risks for personnel and vehicles as well as for the estimation of the quality of the acquired geophysical data (Laake and Insley (2004a and b, Laake and Cutts 2007, Coulson et al. 2009). In turn, geophysical data can be employed to calibrate geophysical characteristics of near-surface layers inferred from satellite imagery.

We distinguish the following types of geophysical surveys :

1. **Frontier exploration** aiming at identification of new basins in large unexplored areas. Satellite imagery can assist defining the outline of potential basins and the definition of scouting surveys.
2. **Structural imaging** focuses on potential structures once the outline and character of a basin has been identified. Satellite imagery can support the design and logistic planning

of geophysical surveys on the ground and can provide estimates for the quality of the acquired data before the data are acquired.

3. **Reservoir characterization** targets the most comprehensive study of the subsurface geological structure and fluids for individual reservoirs and therefore requires the best data quality. Satellite imagery can provide detailed models of the surface and near-surface which provide input to data quality estimation before and during acquisition. For data processing satellite imagery can supply input to processes that correct for noise related to near-surface properties.

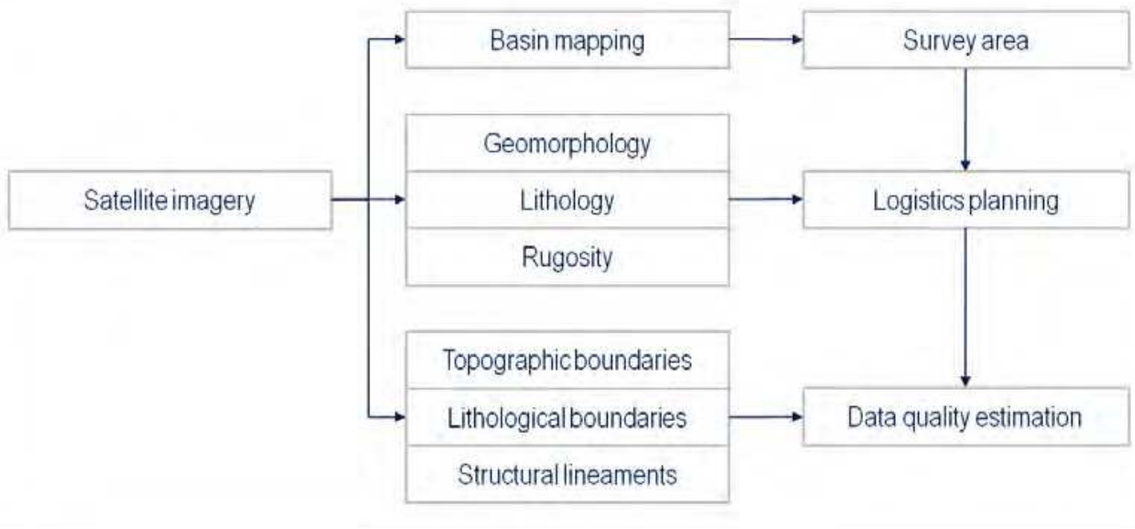

Fig. 15. Workflow for application of satellite imagery to geophysical methods

An outline of the information satellite imagery can provide for geophysical methods and the parameters studied is shown in figure 15. This section focuses on the aspects of survey design and data quality estimation.

The design of geophysical surveys requires an understanding of the logistics and data quality aspects of the target area to correctly estimate the effort required to provide the desired quality of the final subsurface geological product. Satellite imagery can provide the information about the surface and near-surface before the start of the data acquisition (Cutts and Laake, 2009a and b). The method uses satellite imagery to generate geomorphological and litho-structural models of the surface and near-surface as described in the previous section to derive logistic planning and data quality estimation maps.

Figure 16 shows the result of the method for a survey in the Western Desert of Egypt. DEM and multi-spectral data provide topography (fig. 16.a) and lithology class maps (fig. 16.b). The planning of the logistics requires information about limitations for access and maneuver for personnel and vehicles. The terrain classification provides the locations and steepness of escarpments as well as the surface roughness related to hard limestone. The combination of these terrain attributes defines the logistics risk (fig. 16.c). A major obstacle for data quality for this survey is the scattering of seismic waves at the numerous escarpments resulting from the different weathering of limestone and sandstone. Fig. 16.d shows an estimate map for the scatter risk associated with escarpments.

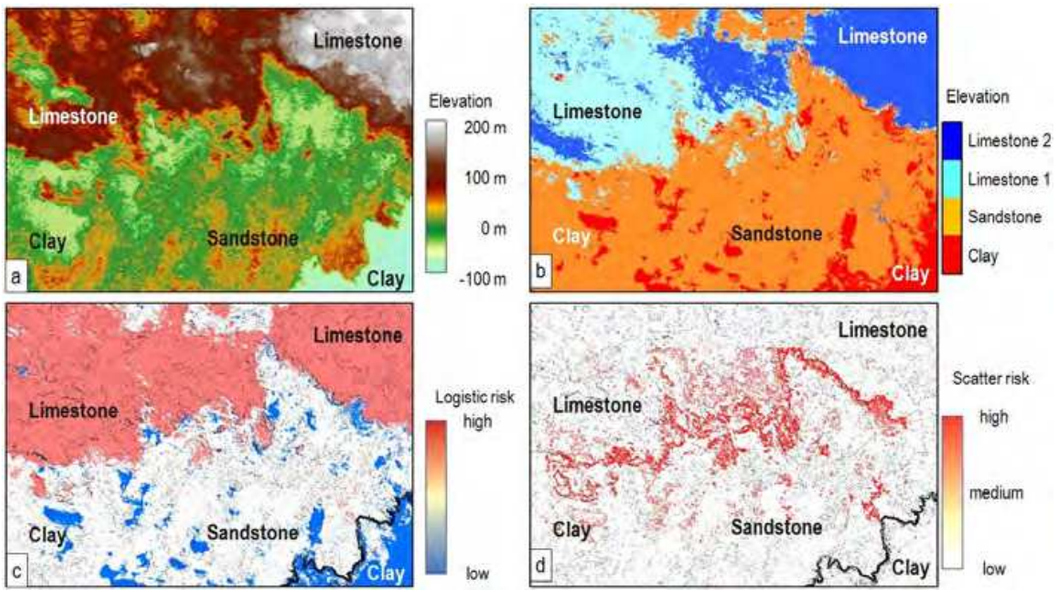

Fig. 16. Survey design based on satellite imagery (Qattara Depression, Egypt) : a – terrain class map based on DEM, b – lithology map, c – logistic risk estimate, d – data quality risk estimate [after Cutts and Laake 2008]

6.1 Logistic planning in volcanic terrain

Vegetation may obstruct the assessment of the logistic risk (Laake 2005b). The basalt plateau close to the Payun Volcano in the Andean foothills of Argentina exposes the risk of big basalt blocks obstructing the access to large areas whereas in other parts of the survey basalt grit exposes no maneuver risk at all (fig. 17.a to c). The analysis of the multi-spectral imagery from ASTER for big basalt blocks is challenging because in both cases – big basalt blocks and bush as well as basalt grit and grass – the ratio of basalt and vegetation is very similar. The resolution of the satellite image of 15 m does not allow the direct mapping of the basalt blocks (fig. 17.d). However, the thermal properties of big basalt blocks are sufficiently different from basalt grit, which allows the discrimination of the basalt block size using the thermal infrared bands from ASTER imagery (fig. 17.e), which is supported by the intermediate back scatter intensity recorded by radar data from Radarsat-1 (fig. 17.f).

6.2 Planning of safe operation in sand dunes

In high sand dunes, both logistics for wheeled vehicles and high absorption for seismic waves may impact the survey design severely (Laake and Insley, 2004a). The analysis of the topography can assist in outlining the dunes and characterizing their shape (fig. 18). Digital elevation models derived from radar or stereo optical data (ASTER in our case) provide the slope index, which can be represented as an index for safe operation. In seismic operation surface gradients above 15 degrees are considered unsafe for operation, whereas in areas with 10 to 15 degrees slope an inspection of the terrain would be advised. Figure 18 shows a composite image of seismic line crossing a dune field. The visible band ASTER image (fig. 18.b) gives a photographic impression of the surface, whereas the DEM (fig. 18.c) provides an impression of the elevations. The slope risk map (fig. 18.d) is obtained from the gradient of the DEM.

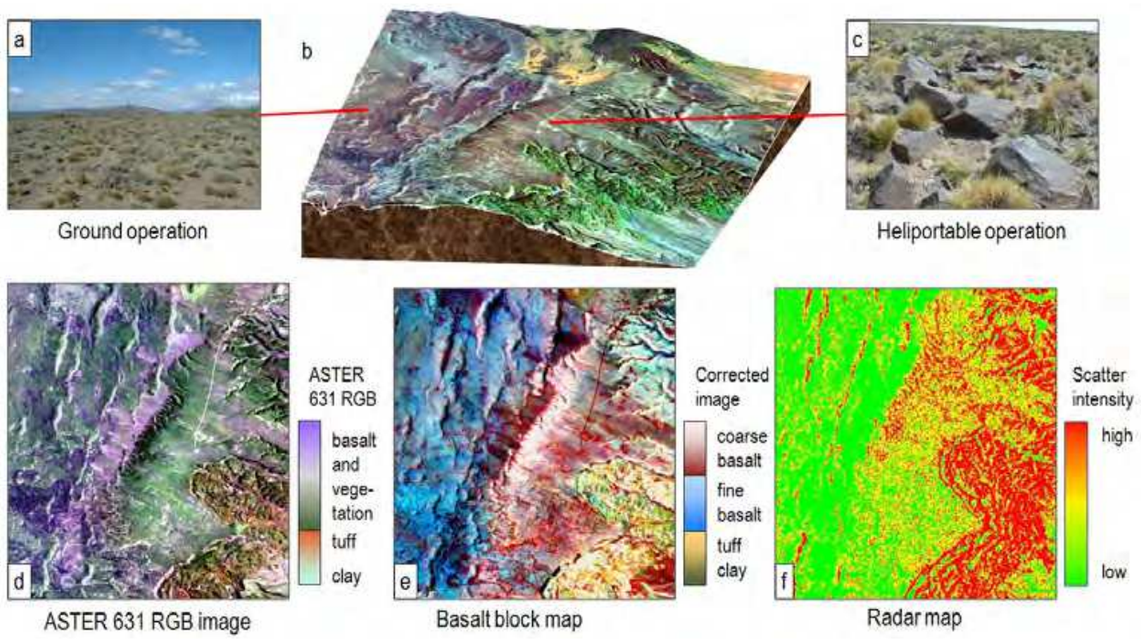

Fig. 17. Satellite imagery based logistic planning in Andean foothills, Argentina : a – basalt gravel plane, b – rendering of ASTER image, c – basalt blocks, d – landuse image [(ASTER 631 RGB], e - basalt block map, f – surface rugosity from Radarsat-1 [after Laake 2005b]

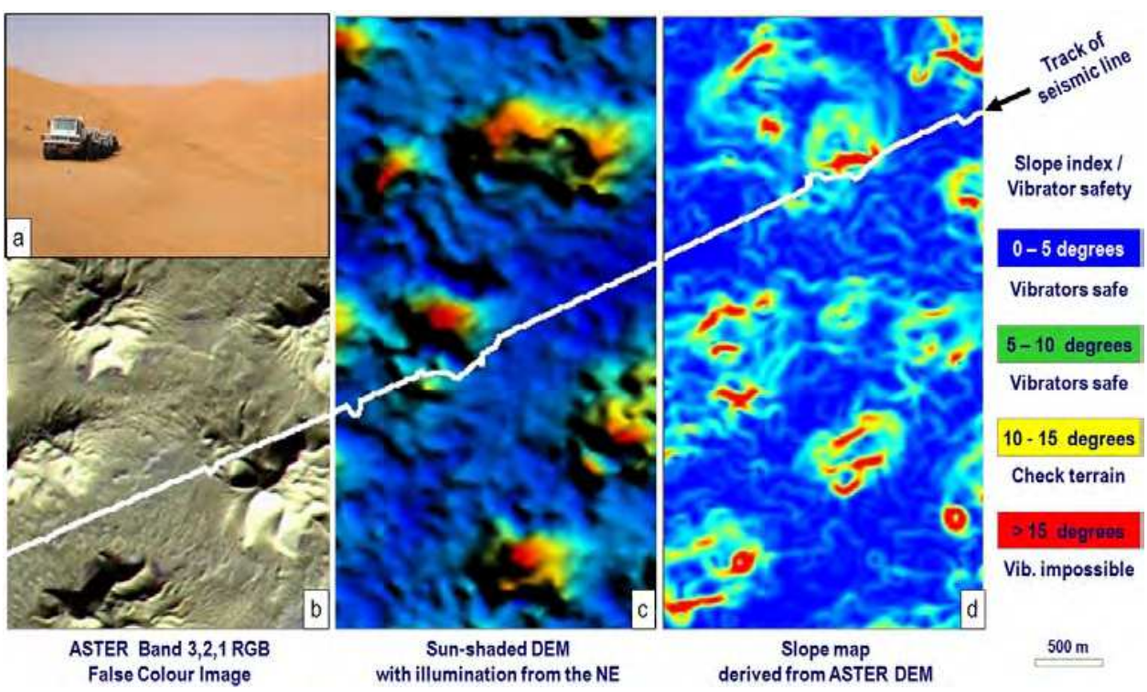

Fig. 18. Planning of safe vibroseis operation in high sand dunes, Berkine basin, Algeria: a – vibrator array in high dunes, b – multi-spectral satellite image [ASTER 321 RGB], c – sun-shaded DEM, d – Slope map derived from DEM [ASTER DEM] [Laake and Insley, 2004a]

6.3 Prediction of accessibility and data quality in sabkha

In arid coastal areas often sabkha called salt flats pose a severe threat to personnel and equipment (Cutts and Laake 2009b). The salt flats may be subject to seasonal inundation, which may change their accessibility significantly. Analysis of the multi-spectral satellite Landsat imagery can allow the detection of halite minerals found in the surface crusts of sabkha. Thermal infrared imagery provides information about the different thermal properties of wet and dry sabkha. The visible band Landsat image in figure 19.b gives an indication of the location of the wet sabkha. The risk that the sabkha surface would not support heavy vehicles (see fig. 19.a) is directly correlated with presence of sabkha and can be derived from a sabkha detection map (fig. 19.c). In addition to its impact on the logistics sabkha also affects the vibrator data quality. High distortion of the vibrator signal, an undesirable data property, is directly related to the presence of sabkha (fig. 19.d).

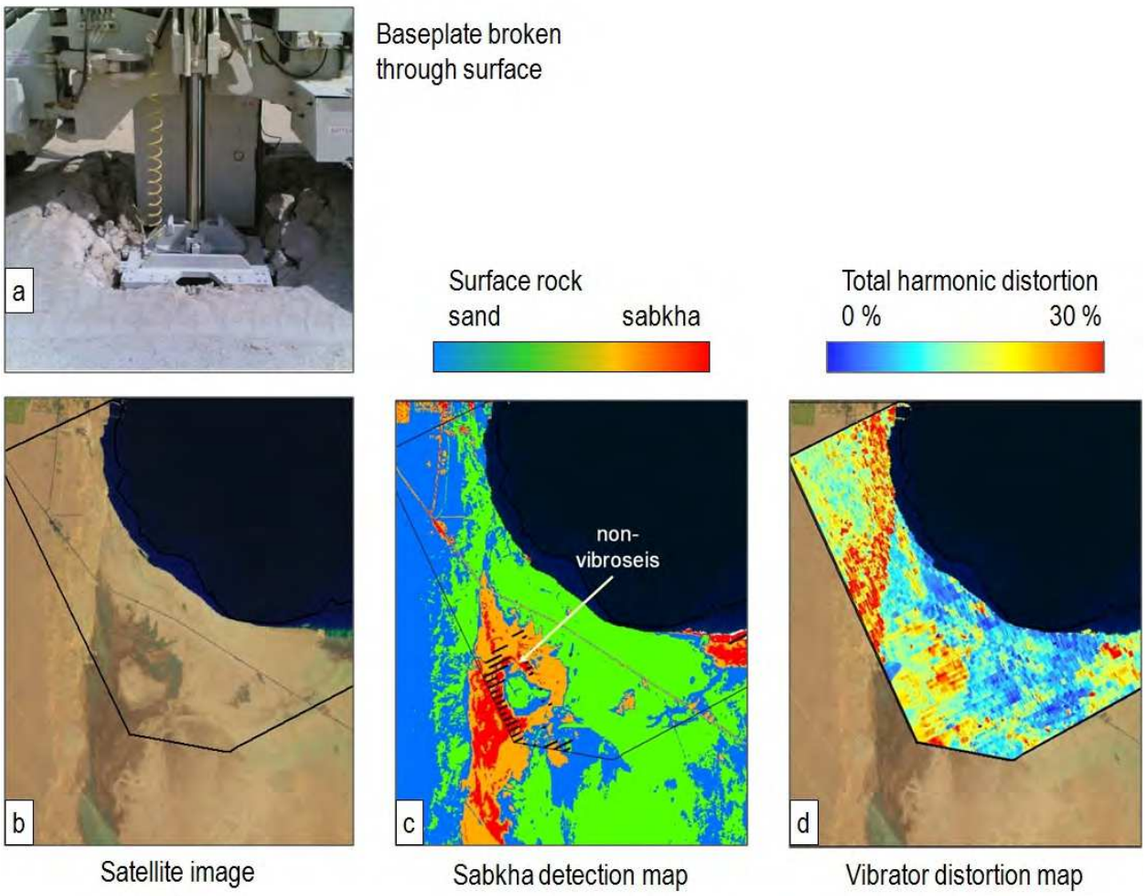

Fig. 19. Prediction of accessibility and data quality of vibroseis operations in sabkha, Sabkha Matti, UAE: a – vibrator baseplate broken through surface crust, b – satellite image [Landsat 321 RGB], c - sabkha detection map, d – map of vibrator total harmonic distortion [after Cutts and Laake 2008]

6.4 Estimation of the vibrator baseplate-to-ground coupling

Hard rock terrain affects the coupling of the vibrator baseplate to the ground (Laake and Tewekesbury 2005). Good ground coupling is achieved when the entire baseplate is in contact with the ground for example on gravel (fig. 20.c). If the baseplate rests on a big boulder, the coupling surface from the baseplate to the ground may be reduced to a very small area resulting in substantial distortion of the transmitted signal and in severe damage to the baseplate (fig. 20.a).

In this case the so-called point loading risk is correlated with hard limestone. The limestone prediction map draped over the DEM is shown in figure 20.b. But even for gravel the ground coupling may be compromised if the force level of the vibrator shaker and the frequency exceed the levels at which the ground supports the weight of the vibrator. The time signal of the baseplate amplitude (fig. 20 bottom) shows the increasing frequency of the shaker force with time along with measured signal distortion. At three moments of the sweep photos of the shaker were taken. As long as the coupling of the baseplate to the ground is perfect the signal distortion is low (fig. 20.d and e). When the ground surface breaks dust is whirled up by the baseplate motion and the distortion goes up (fig. 20.f). Usually frequencies higher than the frequency at which the baseplate breaks through the surface show high phase distortion and deteriorate the data quality. The high distortion for very low frequencies (corresponding to fig. 20.d) is associated with motions of the entire vibrator and are not considered here.

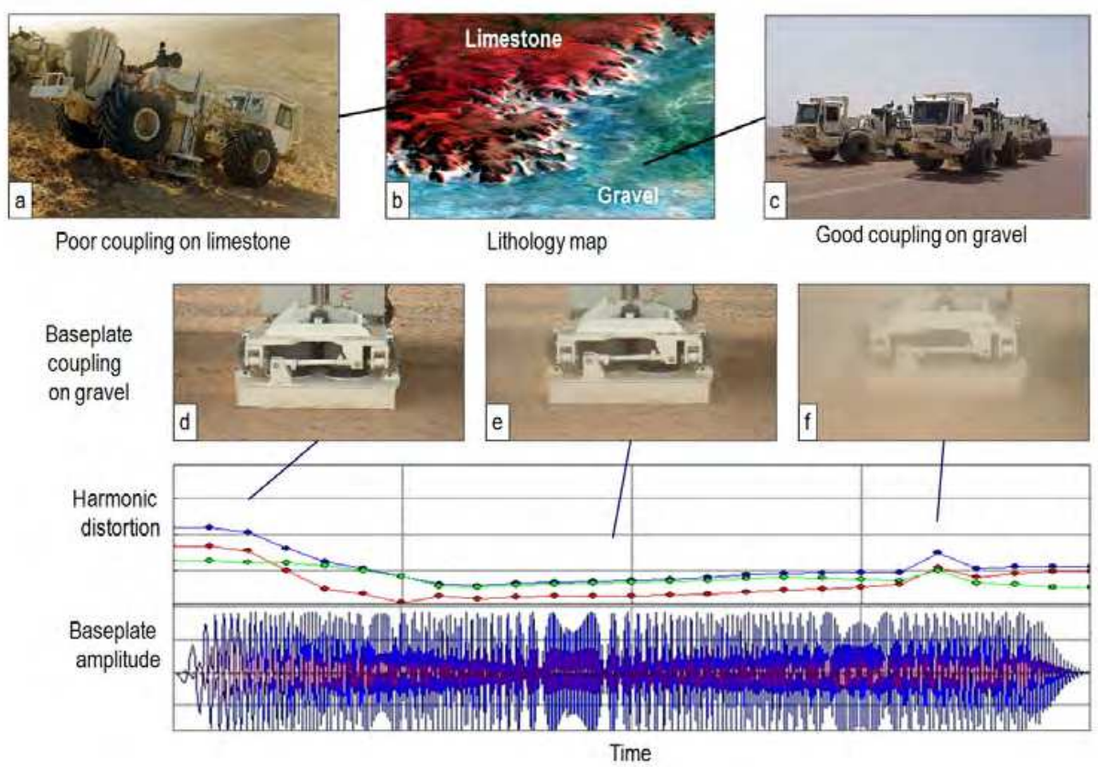

Fig. 20. Prediction of accessibility and data quality for vibroseis operations in hard rocky terrain, Tademait, Algeria: a, c – operations photos, b – virtual 3D lithology map, d - f – photos from baseplate coupling, bottom – baseplate distortion and amplitude time signal [after Laake and Tewkesbury 2005]

Soft terrain may have an impact on both the source coupling as well as on the receiver signal output (Laake 2005a). Due to higher absorption in soft sand, the signal level on sandy surface (fig. 21.b and d) is generally lower than on hard gravel plain (fig. 21.a and c). Satellite imagery can discriminate gravel with shallow evaporite pans on the higher ground from sandy terrain on the lower ground (fig. 21.e). The quality of the source signal also correlates with the terrain character : signals from the sandy terrain show higher distortion (fig. 21.f) and lower ground stiffness (fig. 21.g) than signals from the gravel plain. Interpretation of satellite imagery can provide estimates for the quality of seismic signals obtained from the terrain characterization.

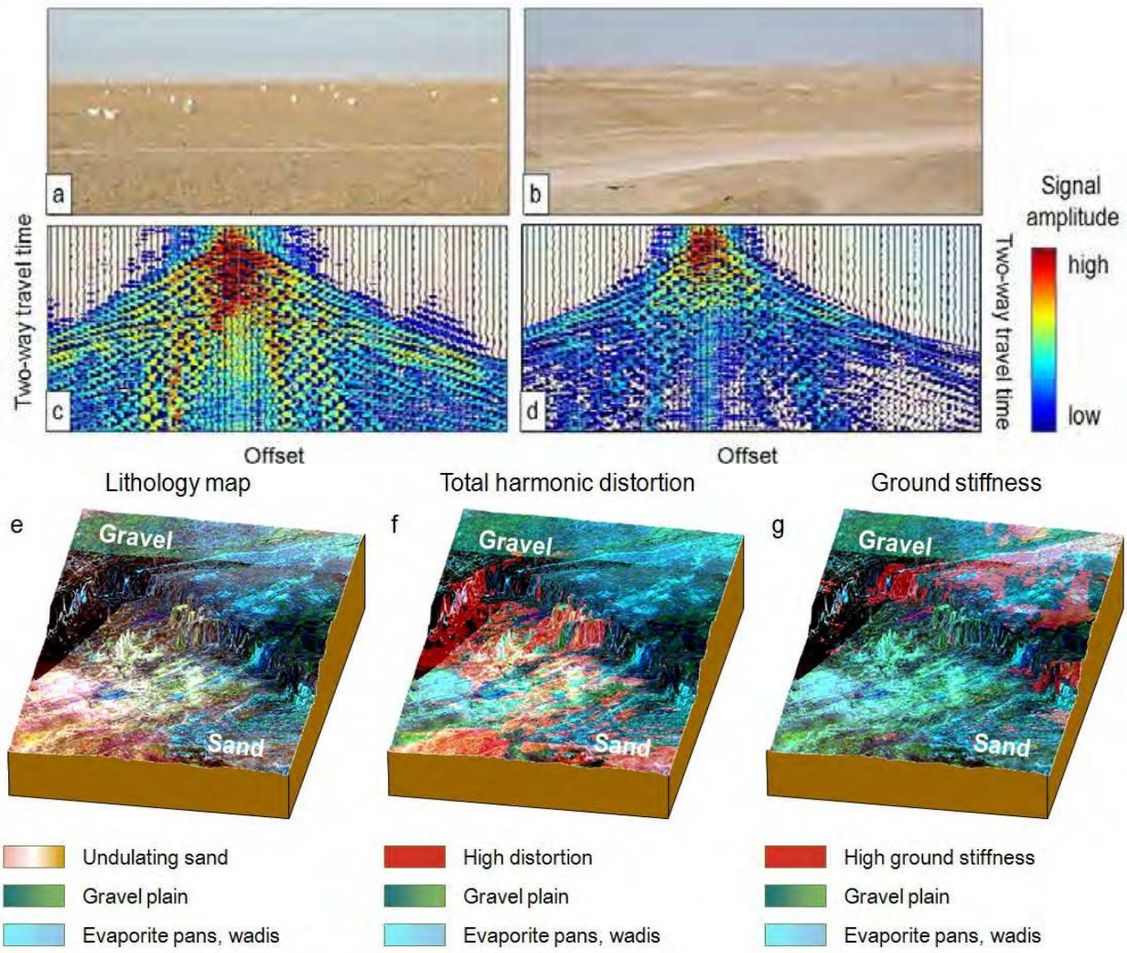

Fig. 21. Correlation of source and receiver data quality with terrain, Kuwait: a – gravel plain, b – undulating sandy surface, c, d – shot record displays, e – surface lithology, f – total harmonic distortion, g – ground stiffness [after Laake 2005a]

6.5 Improvement of static corrections

Near-surface geological models can be generated from the interpretation of satellite imagery for geomorphology and lithology (Laake et al. 2008). Using standardized seismic velocities the geological model is converted into an elastic model, from which estimates for statics corrections can be computed (Laake and Zaghloul 2009). The analysis of the DEM delivers

the topographic classification into three layers (see fig. 22): the platform (sandstone), which occupies most of the study area, as well as the lower platform of the Qattara Depression and the rough higher layer (limestone). The interpretation of the shortwave infrared data reveals that the platform is composed of sandstone, whereas the higher ground consists of limestone (fig. 22 top). When choosing standardized P-wave velocities of 2200 m/s for sandstone and 3300 m/s for limestone we can compute estimated statics values (fig. 22 bottom). The estimated values are compared against refraction static corrections from a 3D seismic survey (fig. 23).

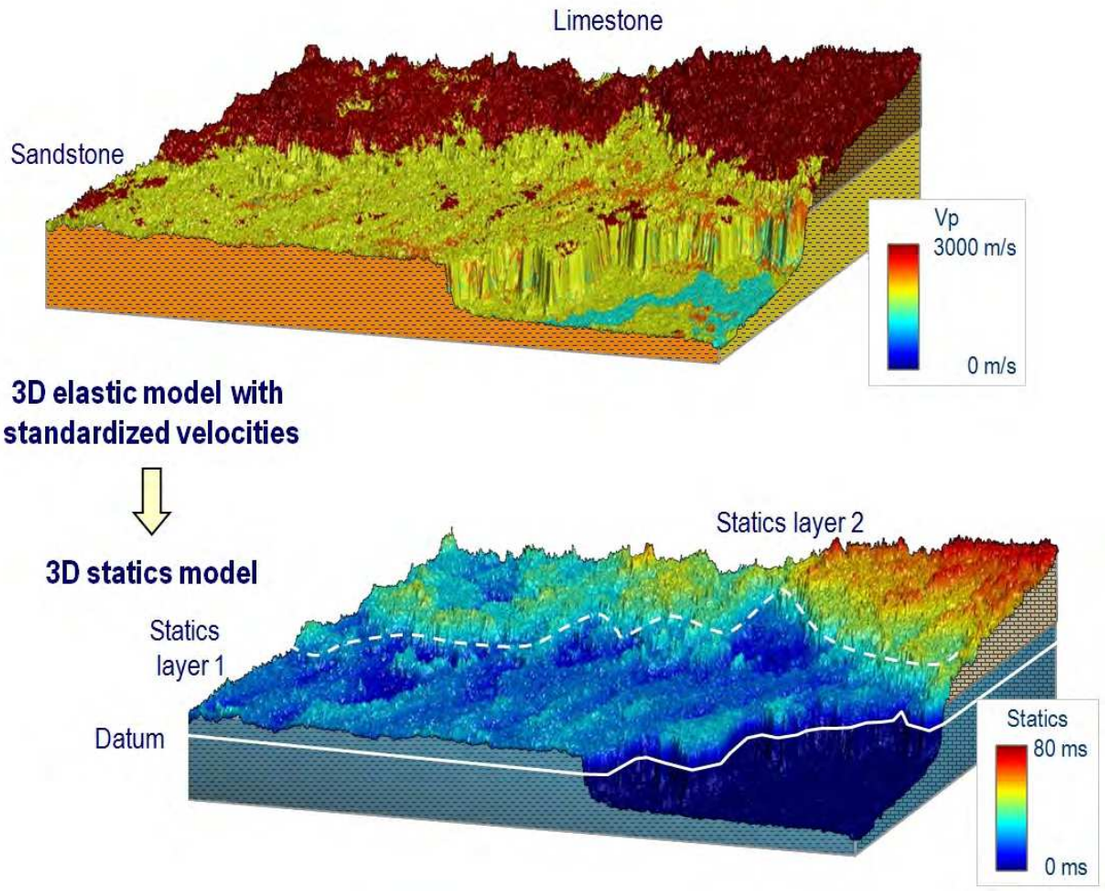

Fig. 22. Estimation of statics corrections from shallow geological model, near Qattara depression, Egypt : top – near-surface geological model from satellite imagery, bottom – 3D statics model [after Laake and Zaghloul 2009]

The static corrections for model 1 (fig. 23.a) use the geological model generated from satellite imagery. The statics contain the lithological details of the sandstone plateau and retain the sharp velocity contrast at the edge of the rough limestone plateau (see fig. 23.c for comparison with the lithology). The statics estimates for model 2 are based on the first break picks from a 3D seismic survey, which are remarkably smoother than the statics from model 1 (fig. 23.d). First break picking involves velocity smoothing over offsets up to 1500 m, which results in a spatial low pass filter. This may result in attenuation of sharp structural lineaments such as fracture zones outcropping at the surface. The difference between the

two models (fig. 23.d) reveals another effect of the spatial smoothing: local velocity anomalies may not be corrected properly and might remain in the data as an artefact, which may lead to the generation of structural artefacts in the deeper seismic data.

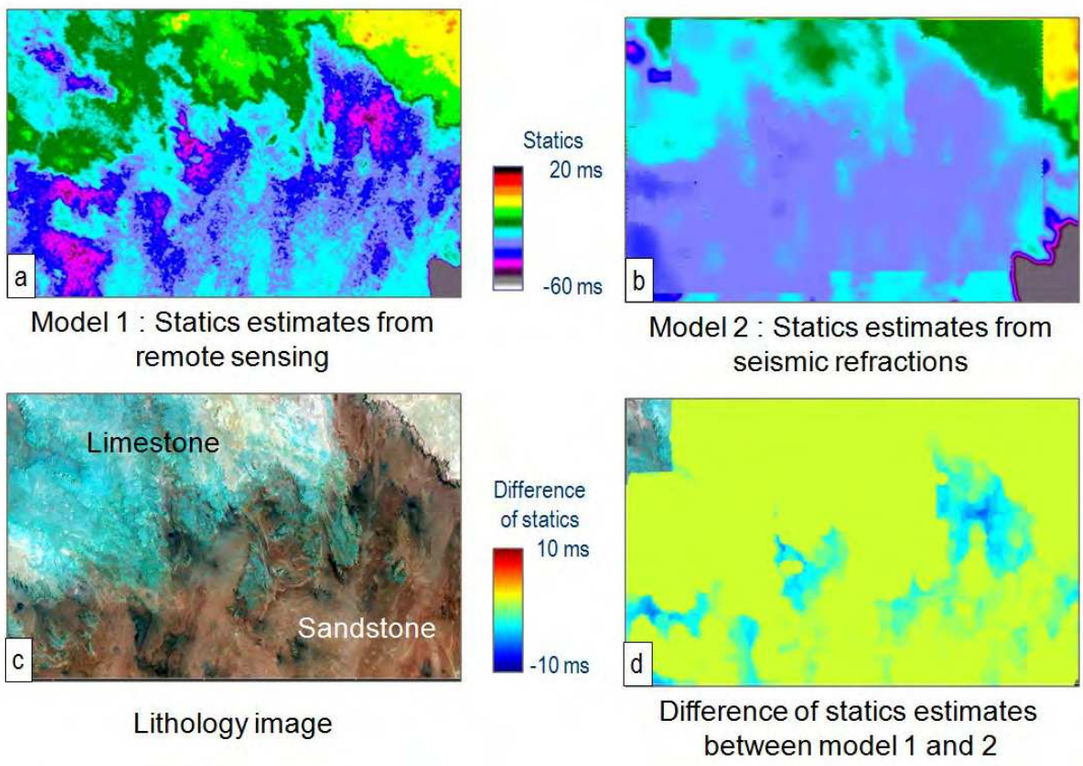

Fig. 23. Comparison of statics from near-surface geological model and from seismic refractions, Qattara depression, Egypt : a – statics corrections from satellite imagery, b – statics from seismic refractions, c – lithology image, d – difference between statics from both models [after Laake and Zaghloul 2009]

7. Consistent deep geological models from data integration

In the final section we will show the benefits of merging interpreted satellite imagery with geological and geophysical data on the western shore of the Gulf of Suez in Egypt by demonstrating the correlation of the geomorphology with the subsurface litho-structure . The processing of multi-spectral imagery from Landsat for lithology and drainage reveals fault structures which are masked by recent wadi deposits (Laake 2010, Laake et al. 2011). The approach follows the idea that tectonic movements deviate the courses of wadis in a characteristic way.

7.1 Mapping of fault outcrops at surface from satellite imagery

The geological setting of the study area is determined by rift faulting in NW – SE direction and transform faults in the perpendicular direction (Darwish and El-Araby 1993, Alsharhan and Salah 1993). The natural colour Landsat 321 RGB image (fig. 24.a) shows the almost featureless beige gravel plain between the Red Sea Mountains in the west and the Gulf of

Suez in the East. The only visible features are SW – NE running wadis delineated through their light sediments. The inverted natural colour image directs the eye to the wadi courses, which reveal several anomalously straight sections (fig. 24.b). When we use all data from Landsat and spectrally enhance the resulting image boundaries along the main tectonic directions are imaged (fig. 24.c): parallel to the coast NW – SE trending linear anomalies point to outcropping parallel fracture zones (dashed lines). The dominating wadi in the southern part of the study area is confined between two straight SW – NE trending lineaments which point to faults running perpendicular to the rift orientation (dotted lines). This map also reveals differences in the mineral composition of the bedrock of the Red Sea Mountain granites. The erosion fans from these two granites may actually be used as tracers to highlight the structural boundaries on the gravel plain. The lineaments are also highlighted in the drainage map, which results from the ratio of the thermal and pan-chromatic bands (fig. 24.d).

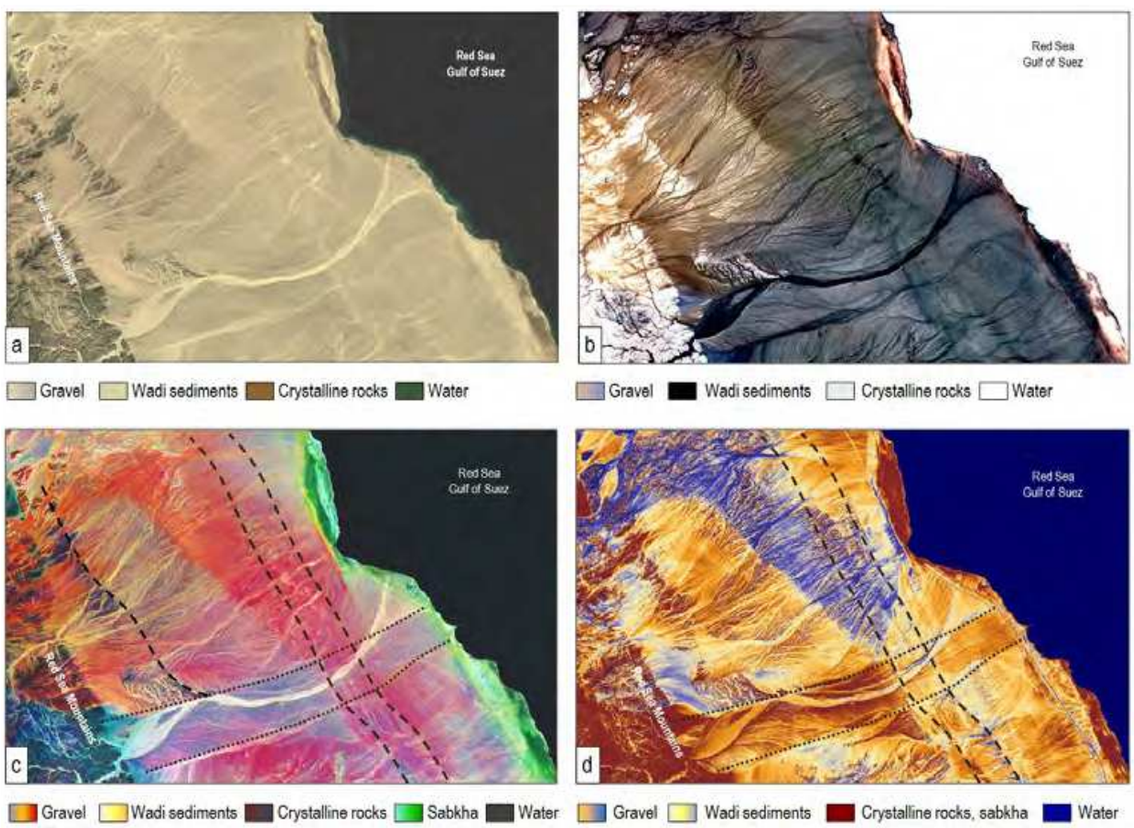

Fig. 24. Surface and near-surface litho-structural mapping from Landsat : a – natural colour image [Landsat 321 RGB], b – inverted natural colour image, c – high-discrimination lithology image, d – drainage map [Landsat bands 6 – 8] [after Laake et al. 2011]

7.2 Mapping of faults in near-surface from shallow geophysical data

In the study area, the fault outcrop pattern mapped from satellite imagery is calibrated with surface features and shallow seismic data from a 3D seismic survey. The only tree in the study area has been found at the intersection of two fault outcrops (fig. 25.a) indicated by the arrow in the lithology map (fig. 25.b). The surface structure becomes evident when

draping the litho-structural map over the vertically exaggerated DEM (fig. 25.c). Arrows indicate the outcrop of faults at the surface. The correlation with faults in the near-surface is achieved by extracting weak zones of low surface wave velocity from seismic 3D data (fig. 25.d). Surface wave velocity analysis provides an iso-velocity horizon which corresponds to a shallow lithologic horizon. This horizon shows very low velocities along the rift parallel fault outcrop zones mapped by remote sensing. In the direction orthogonal to the rift faults a high-velocity structure below the wadi is revealed but no sharp boundaries. This may be due to the transform character of these faults which does not provide an impedance contrast that could be detected from the seismic.

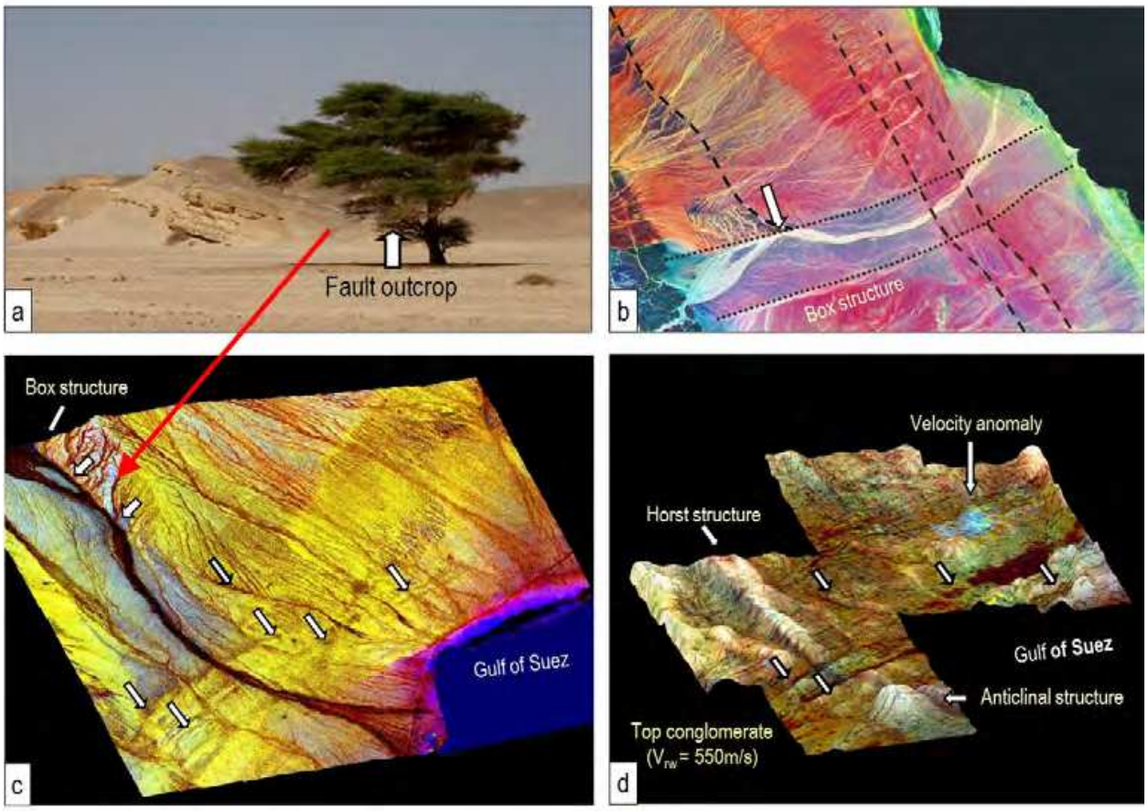

Fig. 25. Calibration of satellite imagery results with near-surface seismic data:
a – tree located at a fault intersection, b – high-discrimination lithology map, c – virtual 3D rendering of the litho-structural map – arrows indicate fault outcrops, d – near-surface formation surface obtained from the velocity analysis of seismic surface waves [after Laake et al. 2011]

7.3 Mapping of faults in the subsurface using surface tamplates

The characteristics of drainage patterns delineated from satellite imagery may also be used to generate shape templates for the detection and extraction of similar structures in subsurface seismic data (fig. 26). We use the drainage map to define the template for a wadi (fig. 26.a) consisting of the braided stream and the fan delta. In our case the braided stream is confined by the SW – NE trending faults perpendicular to the rift orientation, whereas the fan delta part shows so little elevation change that the fan delta crosses the boundary faults (fig. 26.b).

The shape template is used in the processing of the shallow seismic data to search for the correct seismic attribute suited to map the faults which are hidden in most other seismic attributes. In our case the instantaneous frequency attributes were identified for mapping the SE – NE faults because this attribute highlights locally high spectral amplitudes which were interpreted as resonances within the palao-wadi structures (fig. 26.c). Once the shallow paleo-wadi has been identified the same methodology is applied to the deeper data; a total of four paleo-wadis spanning the entire rift history were mapped (fig. 26.d).

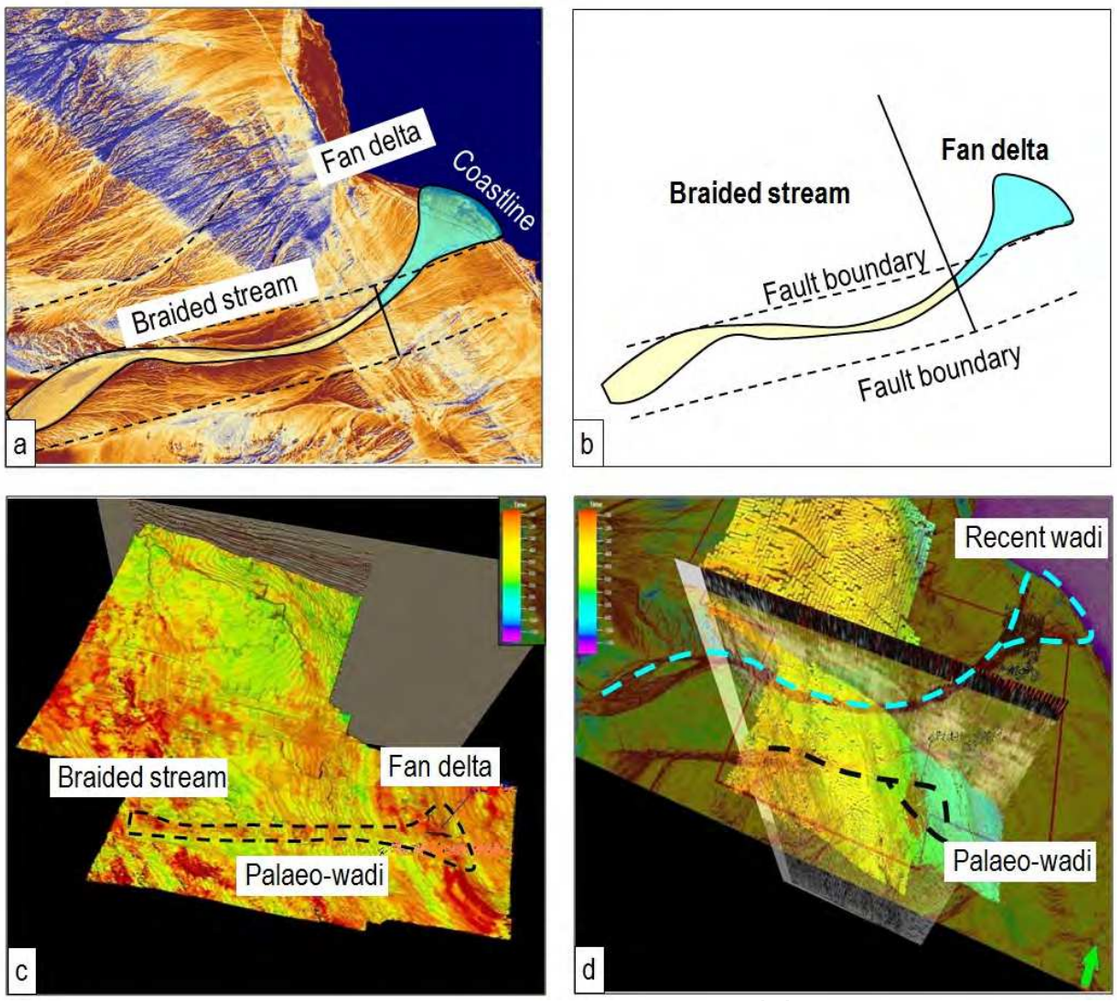

Fig. 26. Satellite based generation of templates for subsurface geobody extraction: a – drainage map, b – extracted wadi pattern, c – detection of similar pattern in shallow seismic data, d – delineation of geobodies in deep seismic data [after Laake et al. 2011]

7.4 Mapping of shallow drilling risk related to faults

Finally the surface and shallow subsurface mapping can be merged into a shallow structural map with indications of shallow drilling risks related to outcropping fault zones (fig. 27). The map basis is a landuse map (Landsat 742 RGB) onto which the near-surface topography is projected. The fault lines delineate areas of shallow drilling risk related to fault induced weak zones, which might lead to collapsing boreholes and/or loss of circulation.

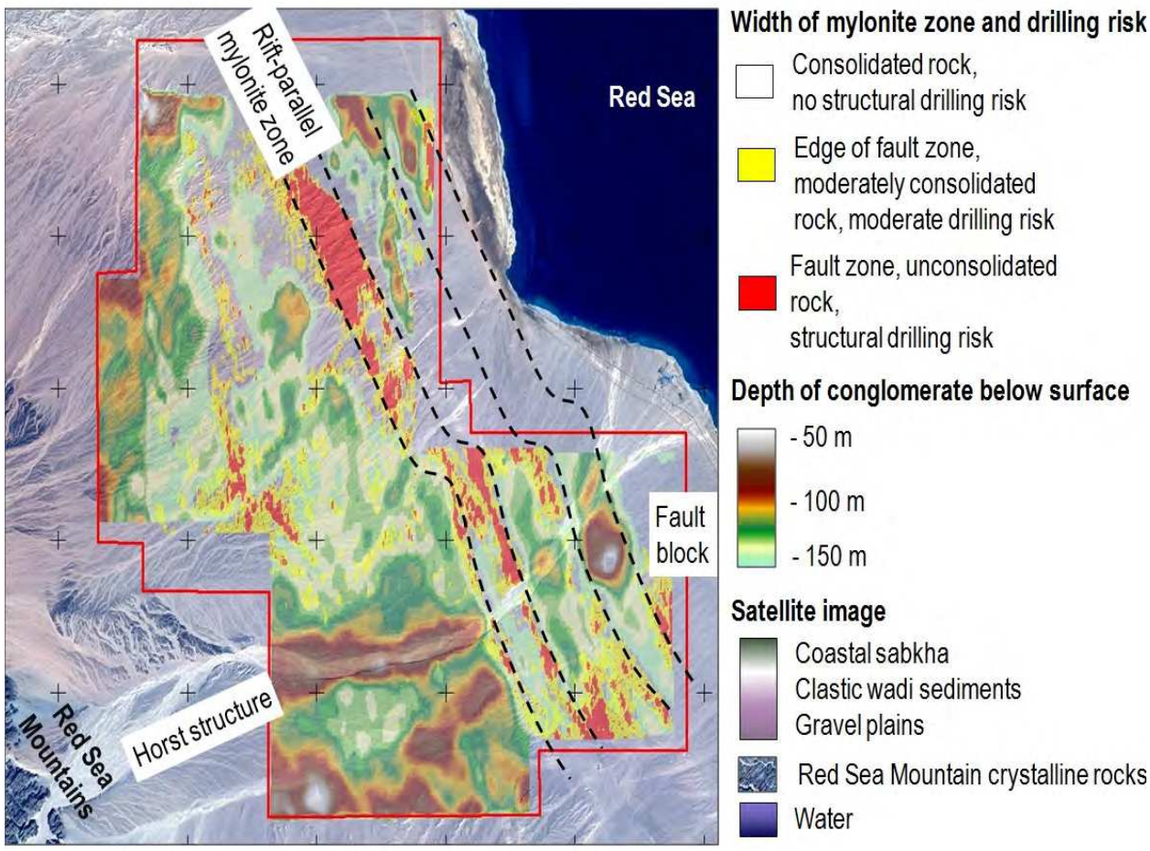

Fig. 27. Shallow structural and drilling risk mapping guided by interpretation of satellite imagery [after Laake et al. 2011]

8. Conclusion

Satellite imagery enables the investigation of the properties of the earth surface in remote areas and over large areas through the mapping of physical properties from satellite based sensors. Optical imagery delivers information about land-use, water features and surface rocks. Microwave radar imagery maps surface roughness when back-scattered at hard surfaces and paleo-drainage when penetrating dry sand cover. Microwave radar distance measurements can be converted into surface topography maps or digital elevation models. The joint interpretation of radar elevation measurements and the geoid shape delivers satellite based gravity anomaly maps, which reflect the thickness of the sedimentary layers above the crystalline basement.

The interpretation of satellite imagery can assist in the planning of surface seismic surveys through assessment of logistic and data quality risks early in the planning specifically when exploring in frontier areas. Interpretation of satellite imagery can provide estimates of the source and receiver data quality and static corrections. Consistent geological models can be generated from the interpretation of satellite imagery for geomorphological and litho-structural properties integrated with geological and geophysical data.

Fig. 28 and table 1 give an overview of the geological features detectable from satellite imagery and their impact on seismic data quality.

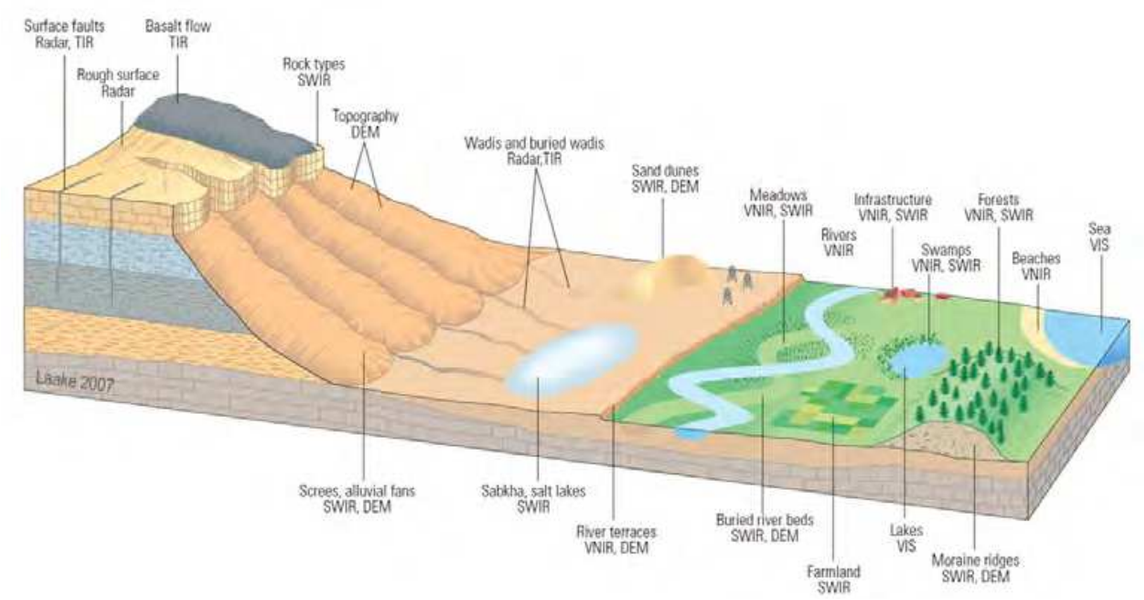

Fig. 28. Characterization of surface and near-surface properties from satellite imagery

Surface Class	Surface Feature	Satellite Imagery	Impact on Data Quality	Impact on Logistics
Topography and texture	Escarpments, river terraces	DEM, radar	Scattering noise	Severe risk for 15 - 25% slope, no access above
	Rough surfaces	Radar	Poor source / receiver coupling	Severe risk of tire damage for vehicles
	Surface faults	TIR, radar	Scattering noise	Only on escarpments
Land use	Swamps, marshes	VIS–NIR	Resonance; velocity statics	If wet, no access for vibrators and vehicles
	Water features	VIS	Special equipment	No vehicle access
Lithology	Basalt flows	TIR	Poor coupling; strong scattering	Often risk for vibrator and vehicle tires
	Claypans	DEM, NIR	Resonance	No access if wet
	Hard rock outcrops	NIR, SWIR, radar	Poor source / receiver coupling	Limited risk of access for vibrators
	Sabkhas, salt lakes	DEM, SWIR	Resonance; velocity statics	Severe risk for vibrator and vehicle access
	Buried rivers	TIR, radar	Velocity statics	No risk
Geo-morph-ology	Moraine ridges	SWIR, DEM	Low velocity, high attenuation	No risk
	Sand dunes	SWIR, DEM	Elevation statics; strong attenuation	Access for vibrators severely limited

Table 1. Detection of surface geological features from satellite imagery and impact on seismic data. For satellite imagery codes see section 3.

9. Acknowledgements

The author thanks ADNOC, Anadarko, Apache Oil Egypt, Bahrain Oil Company, Dara Petroleum Company, Egypt General Petroleum Corporation, Gaz de France, Kuwait Ministry of Oil, Kuwait Oil Company Ltd., Repsol YPF, Sonatrach, TransGlobe Energy, and WesternGeco for the permission to publish the data.
The original data for Landsat 7 ETM+ and MrSID is provided by NASA. The original data for the SRTM DEM is provided by NASA through the CIAT-CSI SRTM website (http://srtm.csi.cgiar.org), the Canadian Space Agency provided Radarsat microwave data. ASTER original data and ASTER GDEM are products of METI and NASA, the original data is property of METI and NASA. Radar based satellite gravity data are provided by the University of California, La Jolla Satellite.
The author also thanks Elisabeth DeTemple, Charles Woodward and Nick Moldoveanu for their reviews, Andrew Cutts for the support with GIS and Claudio Strobbia, Mohamed Sheneshen and Larry Velasco for their contributions to the data integration.

10. References

Alsharhan, A.S. and Salah, M.G. (1995). Geology and hydrocarbon habitat in rift setting: Northern and central Gulf of Suez, Egypt, Bulletin of Canadian Petroleum Geology, Vol. 43, 156–176.

Astakhov, V. I., Svendsen, J. I, Matiouchkov, A., Mangerud, J., Maslenikova, O. and Tveranger, J. (1999), Marginal formations of the last Kara and Barents ice sheets in northern European Russia. Boreas, Vol. 28, pp. 23–45. Oslo.

Coulson, S., Grabak, O., Cutts, A., Sweeney, D., Hinsch, R., Schachinger, M., Laake, A., Monk, D. and Towart, J. (2009). Satellite sensing : risk mapping for seismic surveys, Schlumberger Oilfield Review, Winter 2008/2009, pp. 40-51.

Cutts, A. and Laake, A. (2009). An Analysis of the Near Surface Using Remote Sensing for the Prediction of Logistics and Data Quality Risk, Tunis 2009 – 4th North African/Mediterranean Petroleum and Geosciences Conference & Exhibition, Tunis, March 2009, paper S30.

Darwish, M. and El-Araby, A.M. (1993). Petrography and diagenetic aspects of some siliciclastic hydrocarbon reservoirs in relation to the rifting of the Gulf of Suez. In: Philobbos, E.R. & Purser, B.H. (eds) Geodynamics and Sedimentation of the Red Sea–Gulf of Aden Rift System. Geological Society of Egypt, Special Publication, 1, pp. 155–187.

El-Baz, F. and Robinson, C. (1997), Paleo-channels revealed by SIR-C data in the Western Desert of Egypt : implications to sand dune accumulations, 12th International Conference and Workshops on Applied Geologic Remote Sensing, Denver November 1997.

Guo, H., Lewis, S. and Marfurt, K.J. (2008). Mapping multiple attributes to three- and four-component colour models – A tutorial. Geophysics, Vol. 73, pp. W7–W19.

Jarvis A., H.I. Reuter, A. Nelson, E. Guevara, 2008, Hole-filled seamless SRTM data V4, International Centre for Tropical Agriculture (CIAT), available from: http://srtm.csi.cgiar.org.

Laake, A. (2005a). Application of Landsat data to seismic exploration – Case study from Kuwait, Kuwait First International Remote Sensing Conference and Exhibition, Kuwait September 2005.

Laake, A. (2005b). Remote sensing application for vibroseis data quality estimation in the Neuquen Basin, Argentina, VI Congreso de Exploración y Desarrollo de Hidrocarburos, Mar del Plata, November 2005.

Laake, A. (2009). Hybrid near-surface modeling for seismic property estimation in arctic areas, 71st EAGE Conference & Exhibition, Amsterdam, June 2009, paper T003.

Laake, A. (2010). Enhancing the value of remote sensing data through integration with ground based data in 3D, ESA workshop on satellite earth observation for the oil and gas sector, Frascati, September 2010.

Laake, A. and Cutts., A. (2007). The role of remote sensing data in near-surface seismic characterization, First Break, Vol. 25, pp. 51 – 55.

Laake, A. and Insley, M. (2007). Near-surface characterization from remote sensing data, ENVISAT Symposium 2007, Montreux, April 2007, A457029.

Laake, A. and Tewkesbury, A. (2005). Vibroseis data quality estimation from remote sensing data, Proceedings of the 67th Conference and Exhibition, Madrid, June 2005, Expanded abstracts, paper G017.

Laake, A. and Zaghloul, A. (2009). Estimation of static corrections from geologic and remote-sensing data, The Leading Edge, February 2009, pp. 192-196.

Laake, A., Al-Alawi, H. and Gras, R. (2006). Integration of remote sensing data with geology and geophysics – Case study from Bahrain, GEO 2006, Manama, March 2006.

Laake, A., and Insley, M. (2004a). Applications of satellite imagery to seismic survey design, The Leading Edge, Vol. 23, No. 10, 1062-1064.

Laake, A., and Insley, M. (2004b). Satellite-based seismic technology, World Oil, Vol. 225, No. 9, pp. 27-33.

Laake, A., Sheneshen, M., Strobbia, C., Velasco, L. and Cutts, A. (2011). Integration of 4surface/subsurface techniques reveals faults in Gulf of Suez oilfields, Petroleum Geoscience, Vol. 17, 2011, pp. 165–179.

Laake, A., Strobbia, C. and Cutts, A. (2008). Integrated approach to 3D near-surface characterization, First Break, Vol. 26, pp. 109-112.

Robinson, C.A., Werwer, A., El-Baz, F., El-Shazly, M., Fritch, T. and Kusky, T. (2007), The Nubian aquifer in Southwest Egypt, Hydrogeology Journal, Vol. 15, 2007, pp. 33-45.

Sabins, F. (1996). Remote sensing, principle and interpretation (3rd ed.), Freeman, ISBN 0716724421, New York.

Sandwell, D.T. and Smith, W.H. (2009). Global marine gravity from retracked Geosat and ERS-1 altimetry: Ridge segmentation versus spreading rate, Journal of Geophysical, Vol. 114, B01411, pp. 1-18.

Short, N., (2010), The remote sensing tutorial, NASA 2010, Date of access : 15/06/2011, Available from : http://landsat.gsfc.nasa.gov/about/L7_td.html

Short, N.M.Sr., and Blair, R.W.Jr. (eds.) (1986), Geomorphology from Space, NASA 1986, Date of access : 19/09/2007, Available from : http://geoinfo.amu.edu.pl/wpk/geos/GEO_COMPLETE_TOC.html

USGS (2011), Landsat 7 science data users handbook, Date of access : 24/06/2011, Available from: http://landsathandbook.gsfc.nasa.gov/pdfs/Landsat7_Handbook.pdf

Earth and Environmental Sciences

Edited by Dr. Imran Ahmad Dar

ISBN 978-953-307-468-9

Hard cover, 630 pages

Publisher InTech

Published online 07, December, 2011

Published in print edition December, 2011

We are increasingly faced with environmental problems and required to make important decisions. In many cases an understanding of one or more geologic processes is essential to finding the appropriate solution. Earth and Environmental Sciences are by their very nature a dynamic field in which new issues continue to arise and old ones often evolve. The principal aim of this book is to present the reader with a broad overview of Earth and Environmental Sciences. Hopefully, this recent research will provide the reader with a useful foundation for discussing and evaluating specific environmental issues, as well as for developing ideas for problem solving. The book has been divided into nine sections; Geology, Geochemistry, Seismology, Hydrology, Hydrogeology, Mineralogy, Soil, Remote Sensing and Environmental Sciences.

INTECH
open science | open minds

InTech Europe
University Campus STeP Ri
Slavka Krautzeka 83/A
51000 Rijeka, Croatia
Phone: +385 (51) 770 447
Fax: +385 (51) 686 166
www.intechopen.com

InTech China
Unit 405, Office Block, Hotel Equatorial Shanghai
No.65, Yan An Road (West), Shanghai, 200040, China
中国上海市延安西路65号上海国际贵都大饭店办公楼405单元
Phone: +86-21-62489820
Fax: +86-21-62489821

IntechOpen